

Sizing of Switched Reluctance Machines for Automotive Applications

by
Paul R. Gemin
Professor Ali Keyhani

Mechatronics Laboratory
Department of Electrical Engineering
The Ohio State University
Columbus, Ohio 43210

All Rights Reserved by the Ohio State University

February 13, 2003

ABSTRACT

This research has investigated automotive electrical systems and discussed the need for and requirements of electromechanical actuation and propulsion in modern automotive vehicles. The low cost, easy assembly, and low rotor inertia of the switched reluctance motor (SRM) make it well suited for many automotive applications. One of the drawbacks of SRMs for the automotive industry is the time to market due to the SRMs nonlinear magnetic operation. This research sought to provide a “first pass” design tool for SRM designers. A D^2L sizing equation was developed for SRMs and was programmed in a MATLAB script. Beyond sizing, the MATLAB script also included design guidelines which provide the designer with a complete set of dimensions to model the machine in a more accurate but much more time intensive finite element analysis (FEA) program. The MATLAB script also gives the designer the ability to modify the calculated dimensions and view their effect on output torque.

In developing the sizing program, a large portion of this research was spent investigating maximum and minimum inductance calculations for the SRM. The inductance ratio constant is an important element in the sizing program and cannot be easily determined without some analysis. Three methods for calculating the unaligned inductance were investigated. These methods were implemented and their results compared to experimental and FEA results. None were shown to produce results closer

than 18% for the motor used in this research. Three methods were implemented to calculate the aligned inductance. Two of these were relatively complex and ultimately never produced accurate results. In an effort to understand the problem a third, simple model was created and shown to calculate the aligned inductance with a 4-10% error.

The completed sizing program was verified using speed, torque, current, and efficiency data collected from the studied motor, a 42 V motor capable of providing 2.5 Nm at 4000 rpm. Over the full range of torque, the error between both calculated and measured efficiency and between the calculated speed and measured speed varied from -33% to 20%. This may be an acceptable starting point in some. The sizing program was then used to generate a complete geometry for 3 given points on the SRMs speed torque curve. These results showed considerable variation from the designed machine at higher torques and the reason for this remains to be determined.

Dedicated to my parents

Robert and Sharon Gemin

ACKNOWLEDGMENTS

I wish to thank my adviser, Professor Ali Keyhani, for his insight, support and guidance, which made this work possible.

I would also like to thank Professor Donald Kasten for his many comments and suggestions on this work.

This work has been supported by members of mechatronics lab: Delphi Automotive, TRW, and Emerson Electric. This work has also been supported in part by the National Science Foundation under Grant ECS-0105320.

VITA

February 6, 1978.....Born – Dayton, OH

2000.....B.S.E.E., The Ohio State University

2001-2002.....Graduate Student, The Ohio State University

FIELDS OF STUDY

Major Field: Electrical Engineering

Specialization: Electromechanics, Power Electronics, and Controls

TABLE OF CONTENTS

	<u>Page</u>
Abstract.....	ii
Dedication.....	iv
Acknowledgements.....	v
Vita.....	vi
List of Figures.....	vii
List of Tables.....	viii
Chapter 1	1
Automotive and Switched Reluctance Motor Background	1
1.1 Introduction	1
1.2 Automotive Background	1
1.3 Switched Reluctance Motor Background	3
1.4 Problem Statement	6
Chapter 2	7
Basic SRM Operational Theory	7
2.1 Introduction	7
2.2 Basic SRM Operation.....	7
Chapter 3	13
Theory and Development of the Sizing Equation.....	13
3.1 Introduction	13
3.2 Sizing Equation	13
Chapter 4	18
Sizing Algorithm and Program Input	18
4.1 Introduction	18
4.2 Selecting the Number of Poles and Phases.....	18
4.3 Design Specifications	19
4.4 Sizing Program Algorithm	20
Chapter 5	22
Design Calculations.....	22
5.1 Introduction	22
5.2 Design Guidelines	22
5.3 Calculation of Losses	26
5.4 Reluctance Model Introduction.....	28
5.5 Simple Reluctance Model	30
5.6 Detailed Reluctance Model.....	31
5.7 Corda and Stephenson Unaligned Inductance Model.....	36

5.8	Radun Analytical Inductance Calculations	37
5.9	Simple Aligned Inductance Model.....	38
5.10	Phase and Coil Inductances.....	40
Chapter 6	42
Results	42
6.1	Introduction	42
6.2	Unaligned Inductance Results.....	42
6.3	Detailed Reluctance Model Results.....	44
6.4	Aligned Inductance Model	47
6.5	Sizing Program Verification.....	47
6.6	Sizing Program Dimensions.....	49
Chapter 7	51
Conclusion	51
7.1	Conclusion.....	51
7.2	Future Work	52
APPENDIX A	54
MATLAB Code for Verification of the Sizing Script	54
APPENDIX B	56
MATLAB Code for the First Pass Sizing Script	56
APPENDIX C	59
MATLAB Code to Calculate Aligned Inductances	59
APPENDIX D	61
MATLAB Code for Calculating Unaligned Inductances	61
BIBLIOGRAPHY	63

LIST OF FIGURES

<u>Figure</u>	<u>Page</u>
Figure 1.1: Cross section of a Switched Reluctance Motor.....	4
Figure 1.2: Flux paths showing progression of coil excitation.....	5
Figure 2.1: Coenergy diagram.....	8
Figure 2.2: Instantaneous torque calculation.....	9
Figure 2.3: Energy Conversion Loop.....	11
Figure 2.4: Operating trajectories for saturated and unsaturated operation.....	12
Figure 3.1: Inductance vs. rotor position.....	14
Figure 3.2: Flux linkage vs. current showing inductances.....	14
Figure 4.1: BH curve for Si steel.....	20
Figure 5.1: Lawrenson feasibility triangle.....	24
Figure 5.2: Flux waveforms in SRMs.....	28
Figure 5.3: Simple Reluctance Model.....	31
Figure 5.4 Flux paths for the detailed reluctance model.....	32
Figure 5.5: Detailed reluctance model.....	32
Figure 5.6: Reluctance program flow chart.....	35
Figure 5.7: Flux paths for Corda and Stephenson model.....	36
Figure 5.8: Permeability regions for Corda and Stephenson model.....	37
Figure 5.9: Radun inductance model.....	38
Figure 5.10: Aligned inductance model.....	39
Figure 5.11: Permeability vs. flux density plot and bisection technique.....	40
Figure 5.12: Schematic of one phase with series coils.....	41

Figure 6.1: Comparison of unaligned inductance calculations for several methods	43
Figure 6.2: Percent errors for unaligned inductance calculations.....	43
Figure 6.3: Pole flux densities for the unaligned position	44
Figure 6.4: Pole flux densities for a partially aligned position	45
Figure 6.5: Pole flux densities for the aligned position	46
Figure 6.6: Calculated inductances from FEA and the reluctance models	47
Figure 6.7: Speed calculated from sizing equation compared to experimental data.....	48
Figure 6.8: Efficiency calculated from sizing equation compared to experimental data.....	49

LIST OF TABELS

<u>Table</u>	<u>Page</u>
Table 4.1: Feasible pole/phase combinations	19
Table 5.1: Electrical and magnetic analogies	29
Table 6.1: Sizing equation output comparison	50

Chapter 1

Automotive and Switched Reluctance Motor Background

1.1 Introduction

This section will discuss the evolution of the automotive electrical system which highlights the necessity of continued development of electromechanical systems for improved vehicle efficiency. It will also provide a basic understanding of switched reluctance motor (SRM) operation and how they can be applied to automotive systems.

1.2 Automotive Background

Until 1955 a 6 volt automotive electrical system was the standard [7]. This was sufficient for starting and headlamps but as more accessories were added and engine size increased a change was made to a 12 volt electrical system. Automotive systems are still becoming increasingly electrically oriented. The increasing number of electrical and electronic components will soon exceed the power capabilities of the current electrical system. New systems such as “electrically-heated catalyts to reduce emissions, electromagnetic valve actuators for engines to achieve optimum engine performance and improve fuel economy, electronic switches, high-intensity discharge lamps, electric air conditioners, electric water pumps, and electric and electro-hydraulic power steering” [3]

will improve vehicle performance and efficiency, but the increased load has mandated a new electrical power system.

In an effort to standardize a new system with efficient operation, a push was made for a higher voltage bus. High voltage buses will result in less power losses due to fixed voltage drops of the generator and rectifier components and due to transmission losses. A compromise had to be made between high voltage and safety. In automotive applications, it is desired to keep an open system meaning the voltage must be low enough to ensure human safety without special insulators and connectors. Weighing these points, 42 volts has become the accepted value of the new higher voltage bus. Increasing the bus voltage to 42 volts would decrease the losses due to fixed voltage drops, such as rectifiers, from 15% to 5% which could constitute a fuel economy improvement of 0.5 mpg [8]. Also, an electric power steering system which requires power only when making a turn is estimated to improve fuel consumption by 1 to 3% which corresponds to an improvement of 0.25 to 0.75 mpg depending on vehicle class [8]. These are just a few examples of the benefits of a new higher voltage bus. This change in bus voltage has now allowed the addition of many electric motors to drive system and accessory loads.

Switched reluctance motors could meet many accessory and system requirements mentioned above. Brush type DC motors have long been the choice for accessory system motors. This is because the automotive industry is largely a cost driven industry and brush type DC motors are inexpensive because they require little drive circuitry, are relatively simple to manufacture, and have a short design time due to simpler design

considerations. Brush type motors do have the drawback of higher losses due to the brush contact point. This sliding contact also becomes a wear issue. Now that semiconductor switches are becoming less expensive motors that require electronic commutation, such as brushless DC motors and SRMs, are viable options in the automotive industry.

SRMs could also be used for vehicle propulsion. Several automakers now offer production hybrid vehicles. Hybrid vehicles use a combination of an internal combustion engine and an electric motor to provide peak torque when needed but also to provide efficient constant speed driving. The advantages and disadvantages of SRMs compared to other motor types for automotive applications will be discussed in the following section.

1.3 Switched Reluctance Motor Background

The basic concept of the switched reluctance motor has been known for quite some time with the earliest recorded switched reluctance motor being built in 1838. The motor was used to power a train on the Glasgow-Edinburgh railway in Scotland [1, 9]. An SRM is a doubly salient structure with windings only on the stator. Figure 1.1 from [15] shows a cross section of the rotor and stator of an 8/6 machine (a motor with eight stator teeth and six rotor teeth).

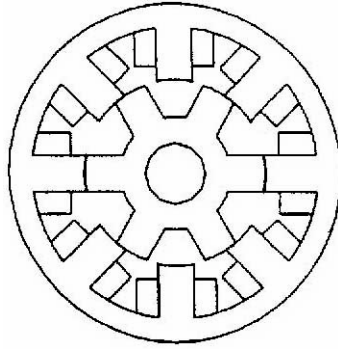


Figure 1.1: Cross section of a Switched Reluctance Motor

Many different configurations exist but the details of those will not be discussed here. The basic operation consists of powering coils on diametrically opposed stator teeth. This will cause the rotor teeth to align themselves to create a path of minimum reluctance or maximum inductance. Once the rotor and stator teeth are aligned the phase current is shut off and the next set of coils is powered. This progression is shown in Figure 1.2 from [15]. The darker stator poles in the picture are the energized poles. The rotor movement and progression of energized poles can be seen. Note that the rotation of the rotor is in the opposite direction of the coil progression for the 8/6 case.

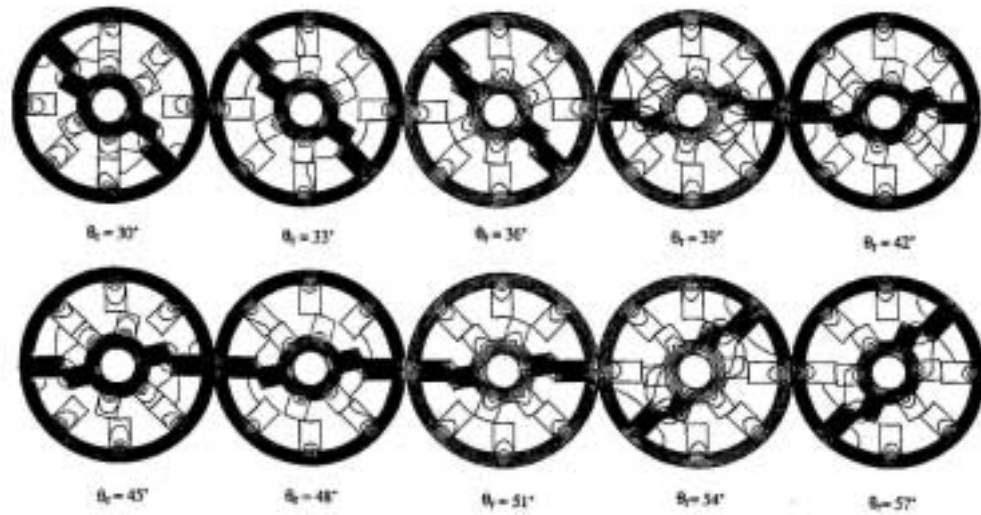


Figure 1.2: Flux paths showing progression of coil excitation

SRMs are becoming increasingly prominent due to advances in power electronics. SRMs are less expensive to construct than most motors because they do not require any electrical connection to the rotor or permanent magnets and the stator windings can be easily pressed over a pole.

Since SRMs lack windings or permanent magnets on the rotor they have a low rotor inertia and can be accelerated very quickly. This has led to their application as control surface actuators in airplanes and experiments with braking in automobiles [2]. Both of the applications listed above also require an actuator with a high fault tolerance which the SRM meets. In an SRM each phase is independent and the motor could still operate without a phase.

SRMs do suffer from high torque pulsations and acoustic noise. The torque pulsations are due to alignment with a small number of stator teeth. The number of stator teeth could be increased to lower torque pulsations but this requires more phases and also diminishes the average torque because the teeth become closer together and the ratio between aligned and unaligned inductance drops. The torque pulsations are one source of the acoustic noise but the major source is from radial forces which deform the stator. Designing a more rigid stator can combat this deformation but it cannot be eliminated making the SRM an inherently noisy motor.

One of the major difficulties associated with SRMs is design. The SRM's airgap is not consistent which causes difficulty in calculating airgap flux densities and saturation in the rotor and stator steel. In fact, the saturation of the steel further complicates airgap flux density calculations. This complicates torque and power calculations which are necessary for determining the size of the machine.

1.4 Problem Statement

This thesis proposes to develop a program for quickly determining "first pass" machine dimensions for a switched reluctance machine. These dimensions can be used to compare the SRM to other machine types such as permanent magnet or induction motors in order to determine which is best suited for an application. The dimensions can also be used as a starting point for the SRM's design in a finite element analysis (FEA) modeling program.

Chapter 2

Basic SRM Operational Theory

2.1 Introduction

This chapter will provide the theory necessary for understanding SRM operation. The material covered in this chapter will relate to the development of the sizing equation covered in Chapter 3 and also to design considerations which will be covered in Chapters 4 and 5.

2.2 Basic SRM Operation

In a switched reluctance motor torque is produced when coils on diametrically opposed, salient, stator teeth are energized. This causes the salient rotor poles to align itself with the stator teeth in a position of minimum reluctance or maximum inductance. Note that because the rotor has no magnetic sources the stator current direction is not related to the direction of torque. Torque is always produced in the direction of the nearest aligned position.

Torque can only be produced in the direction of increasing inductance. This means that at least two phases are required to generate torque at all rotor positions in a symmetric motor [8]. As a coil is energized and a stator and rotor pole begin to overlap

local saturation of both stator and rotor poles occurs. This nonlinearity necessitates that torque must be computed in terms of the co-energy, W , which takes into consideration the flux linkage's dependence on both rotor position and phase current..

$$T(\theta, i) = \frac{\partial W(\theta, i)}{\partial \theta}$$

Where θ is the rotor position and i is the coil current. Thus the torque depends on both the current and rotor position.

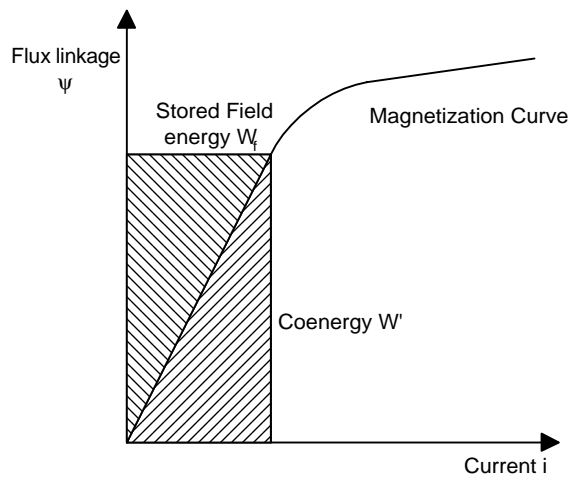


Figure 2.1: Coenergy diagram

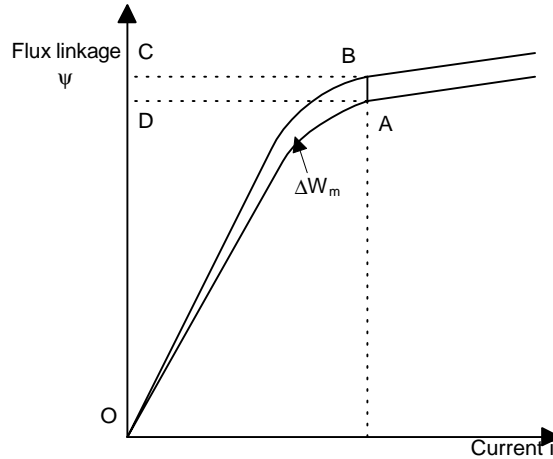


Figure 2.2: Instantaneous torque calculation

The coenergy diagram in Figure 2.1 above is used to describe the calculation of instantaneous torque. The following example is taken from [9]. It illustrates a simple calculation of the conversion of energy from the supply to mechanical work. The term, ΔW_e , represents the change in electrical energy from the supply.

$$\Delta W_e = ABCD$$

Here ΔW_f represents the change in stored field energy.

$$\Delta W_f = OBC - OAD$$

Finally the change in mechanical energy is calculated.

$$\begin{aligned} \Delta W_m &= T\Delta\theta \\ &= \Delta W_e - \Delta W_f \\ &= ABCD - (OBC - OAD) \\ &= (ABCD + OAD) - OBC \\ &= OAB \end{aligned}$$

This illustrates that some of the supply energy is converted to mechanical work while some of the energy is stored in the magnetic field. The energy stored in the field is not available for work but it is instead returned to the supply. This is analogous to an AC motor operating at a lagging power factor.

$$\psi = \int (V_s - Ri)dt = \frac{1}{\omega} \int (V_s - Ri)d\theta$$

If the phase resistance, R , is assumed small and the supply voltage, V_s , is assumed constant then the flux linkage, ψ , will increase linearly with rotor position. Figure 2.3a shows that the current rises linearly at first while the unaligned inductance stays relatively constant. Then as the poles overlap the inductance rises producing a back emf and limiting the current. This is referred to as the fluxing period. In figure 2.3b the phase is commutated meaning the supply voltage is reversed and the current freewheels through the freewheeling diode. This is called the de-fluxing period. At the point of commutation the total energy is equal to the sum of the mechanical energy, W_{mt} , and the stored field energy, W_{fc} . After commutation the energy, W_d , is returned to the supply and sum energy W_{md} is converted to mechanical work but it is less than half of W_{fc} . At this point no current flows and no flux is produced by the phase. Figure 2.3c shows the complete energy conversion loop.

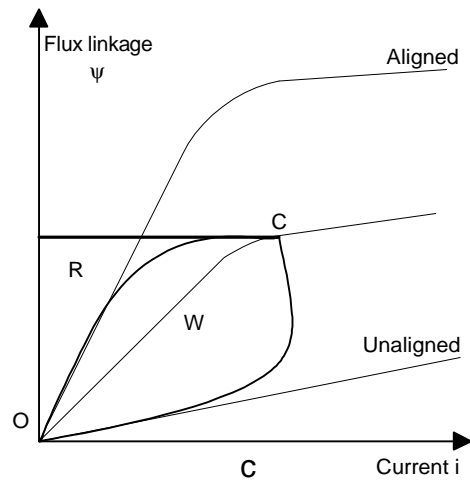
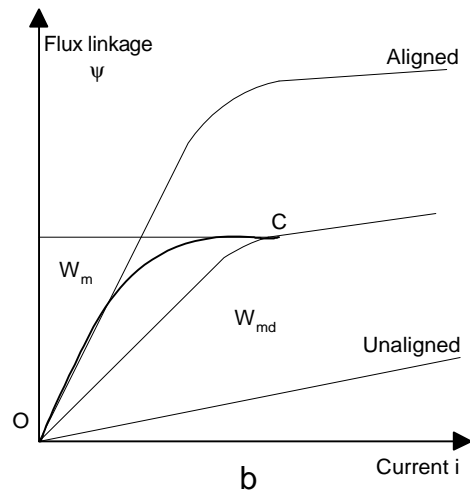
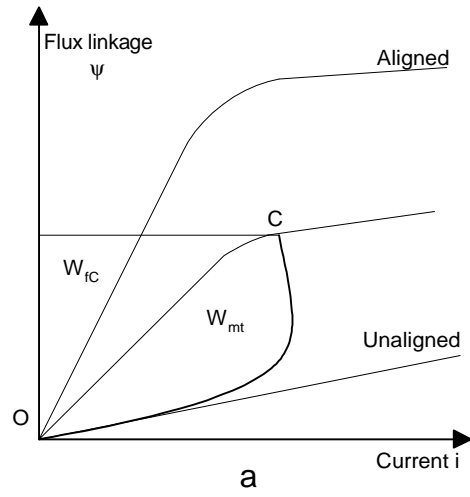


Figure 2.3 Energy Conversion Loop

Radun [12] points out the importance of saturation in an SRM. This is illustrated in Figure 2.4. It can be seen that the energy converted in Operating Trajectory 1 where the teeth do not saturate is only about half that of Operating Trajectory 2 where local saturation occurs.

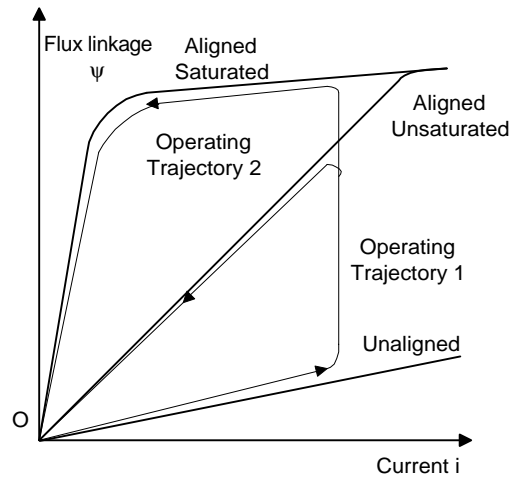


Figure 2.4: Operating trajectories for saturated and unsaturated operation

Chapter 3

Theory and Development of the Sizing Equation

3.1 Introduction

This chapter provides the theory necessary for the development of a sizing program. Though a sizing equation is intended to provide the user with machine dimensions, a sizing program will still require many design inputs which the user will have to select. This chapter will only discuss what must be known in order to use the sizing equation. Chapters 4 and 5 will address the selection and calculation of initial values to use in the sizing equation.

3.2 Sizing Equation

Figure 3.1 shows the inductance change with rotor position. This property is the basis for SRM operation. It should be noted that as the phase current is increased the peak aligned inductance will decrease due to saturation in the steel but the unaligned inductance will stay the same. In the unaligned case the reluctance is so high – due to the large airgap – that the steel will not reach saturation.

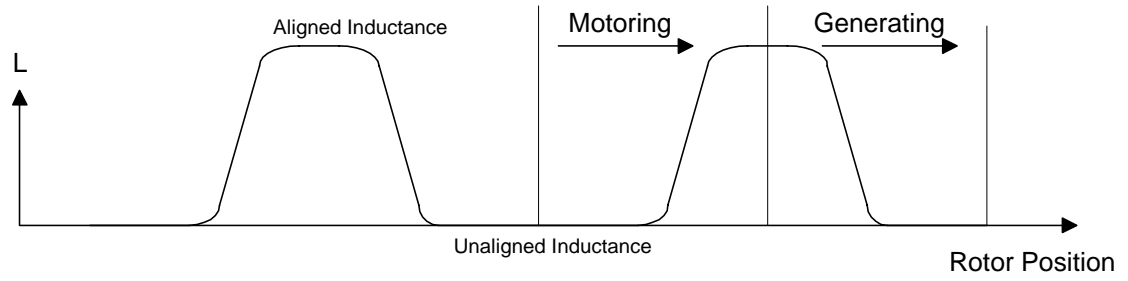


Figure 3.1: Inductance vs. rotor position

Figure 3.2 shows another diagram of flux linkage versus current. In this case the slopes of the lines drawn are inductances. The inductances on this figure were used in the derivation of the sizing equation for the SRM.

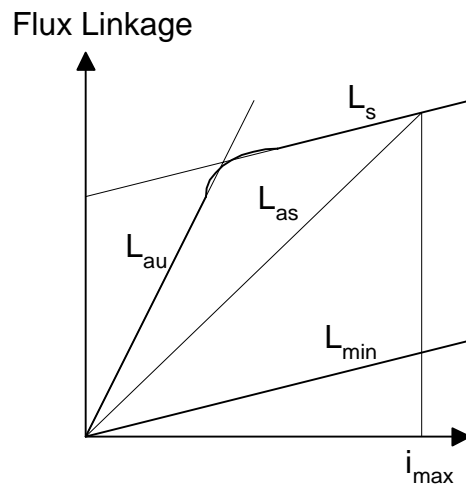


Figure 3.2: Flux linkage vs. current showing inductances

For Figure 3.2, L_{\min} is the unaligned inductance, L_{au} is the aligned unsaturated inductance, and L_{as} is the aligned saturated inductance.

First a saturation factor is calculated.

$$\sigma = \frac{L_{as}}{L_{\min}}$$

Then an unsaturated inductance ratio is calculated.

$$\lambda_u = \frac{L_{au}}{L_{\min}}$$

When a phase is conducting the basic equation of operation follows.

$$V = iR + \frac{d\psi}{dt}$$

This can be integrated from minimum to maximum inductance assuming a linear slope as shown in Figure 3. Also, the resistance is relatively small and is ignored. Thus:

$$V = \frac{d\psi}{dt}$$

$$\Delta\psi = (L_{as} - L_{\min})i$$

$$\Delta t = \frac{(\theta_{off} - \theta_{on})}{\omega} \approx \frac{Stator_Pole_Arc}{\omega} = \frac{\beta_s}{\omega}$$

Combining these result gives an expression for voltage.

$$V = \frac{(L_{as} - L_{\min})i\omega}{\beta_s} = \frac{\omega}{\beta_s} iL_{as} \left(1 - \frac{1}{\sigma\lambda_u}\right)$$

At maximum inductance the flux linkage:

$$\psi = L_{as} i = N\Phi = NB_s A_s$$

where B_s is the average flux density in the stator pole at the L_{\max} position and A_s is the cross sectional area of the stator pole. A_s is calculated below when β_s is small.

$$A_s = 2 \frac{D}{2} \sin\left(\frac{\beta_s}{2}\right) L \approx \frac{D\beta_s L}{2}$$

Now the sizing equation constant K_2 is defined. K_2 provides a relationship based on steel saturation and maximum and minimum inductance.

$$K_2 = \left(1 - \frac{1}{\sigma\lambda_u}\right) = 1 - \frac{L_{\min}}{L_{as}}$$

With all the constants now defined the voltage equation can be written again.

$$V = \frac{1}{2} \omega N B_s D L K_2$$

The overall sizing equation must be based on the power of the machine.

$$P = K_d V I \eta$$

In the above equation η is the machine efficiency. K_d is the duty cycle and I is rms phase current defined below.

$$K_d = \frac{m\theta_c N_r}{2\pi}$$

$$I = \frac{i}{\sqrt{m}}$$

In the above equations m is the number of phases.

Next K_B is defined as a ratio between the max flux density in the teeth and the average flux density in the air gap, also called the magnetic loading.

$$K_B = \frac{B_s}{B}$$

Then the electrical loading is defined. This value is in ampere turns per meter. This is the ampere turns distributed over the circumference of the airgap.

$$Q = \frac{2NI}{\pi D}$$

This allows the equation for power to be written again.

$$P = K_d K_B K_2 \omega \eta B Q \frac{\pi D^2 L}{4}$$

In most cases the desired power is known and the size must be determined so the equation can be rearranged to solve for length.

$$L = \frac{T}{K_d K_B K_2 \eta B Q \frac{\pi}{4} D^2}$$

D must still be input but often a maximum value can be set on this.

Several terms of the sizing equation require substantial computation to determine. The efficiency will require much computation to determine iron, copper, and friction and windage losses. The inductances of the machine must be known in order to determine K_2 and the flux densities at various points in the machine must be known in order to determine K_B .

Chapter 4

Sizing Algorithm and Program Input

4.1 Introduction

As stated in Chapter 3, the sizing program will still require many design inputs which the user will have to select. This chapter will cover the initial design decisions which must be made and the tradeoffs associated with these decisions. This chapter will also introduce the sizing algorithm implemented in a MATLAB script.

4.2 Selecting the Number of Poles and Phases

The first design decision to be made is the number of poles and phases. Single phase and two phase SRMs are impractical unless eccentricities are designed into the rotor to guarantee starting in any position. Many of these designs are discussed in [9] but they will not be covered here. Three phase motors are the most common.

One of the most critical tradeoffs is that as the number of poles are increased the motor provides smoother torque but the inductance ratio will be lower indicating a lower peak torque and thus a lower torque density.

Higher phase numbers require more power electronic components but allow the torque ripple to be reduced while not lowering the inductance ratio and thus the torque density of the motor.

A table has been provided which indicates possible pole and phase combinations. More details can be found in [9].

m	Ns	Nr	multiplicity	stroke angle	strokes/rev
1	2	2	1	180	2
2	4	2	1	90	4
3	6	2	1	69	6
3	6	4	1	30	12
3	6	8	1	15	24
3	12	8	2	15	24
3	18	12	3	10	36
3	24	16	4	7.5	48
4	8	6	1	15	24
4	16	12	2	7.5	48
5	10	4	1	20	18
5	10	6	1	12	30
5	10	8	1	9	40
5	10	8	2	18	20

Table 4.1: Feasible pole/phase combinations

4.3 Design Specifications

The designer must also specify the desired machine torque at given speed.

Normally a constraint will be placed on either the machine length or the machine outside diameter in order to determine the other dimensions. The properties of the steel used will also have to be specified. The BH saturation curve of the steel used is important for all

inductance and torque calculations as was explained in Chapter 3. Figure 4.1 shows a sample BH curve for a Silicon steel.

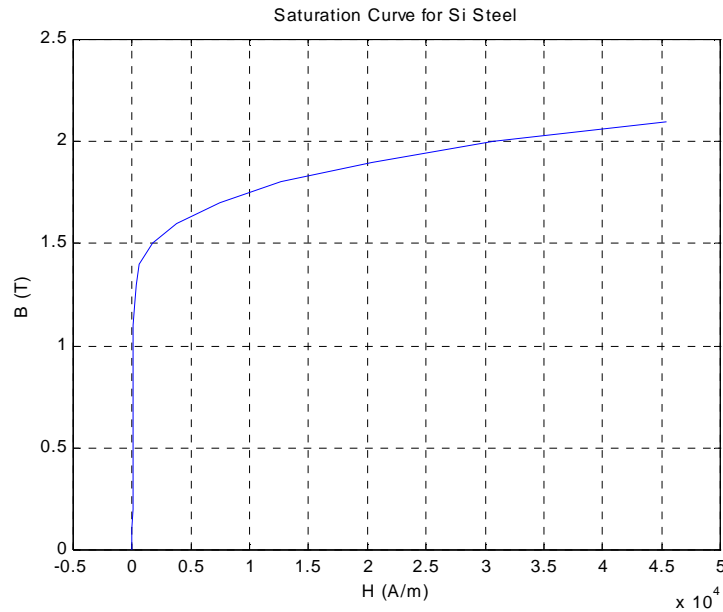


Figure 4.1: BH curve for Si steel

4.4 Sizing Program Algorithm

This section will discuss the algorithm that has been implemented to determine the required size of an SRM. Some of the necessary topics have already been presented and these allow for the algorithm to be developed. Other topics will be covered in later chapters but this discussion illustrates their eventual place in the overall program.

First the user must input the number of poles and phases as well as material properties and a size constraint (either length or diameter) of the machine. Then guidelines which will be covered in Chapter 5 will be used to choose initial dimensions.

Then a guess is made to select an initial value for K_2 . It falls in a range from .65-.9 [4]. Then the sizing equation from Chapter 3 will use all above info to calculate a machine length or diameter. This length or diameter combined with all other dimensions will be used to calculate a value for K_2 and B_s . The new values of K_2 and B_s are then used in the sizing equation to calculate torque. All calculated machine dimensions are then output. The dimensions calculated will be for a machine whose torque capabilities may be less than or more than specified by the user. This will depend on how closely the initial guess for K_2 and B_s compare to the calculated values. With an understanding of the sizing equation the user can modify output dimensions to increase or decrease the torque.

Chapter 5

Design Calculations

5.1 Introduction

This chapter will discuss guidelines for the design of SRM. Some of these guidelines are developed from theory while others are based on successful machine designs. These guidelines are primarily used to determine internal dimensions which are used in the calculation of K_2 and B_s in the final sizing program. These guidelines could be modified in the MATLAB script as a designer gains experience.

This chapter also discusses the calculation of K_2 and B_s which was a significant portion of this research. Several methods are discussed and their results will be discussed in Chapter 6.

5.2 Design Guidelines

5.5.1 Airgap

A small airgap is required to keep a high aligned to unaligned inductance ratio and to minimize the volt-ampere requirement of a motor drive. Airgaps less than 0.25 mm may require post assembly machining to avoid interference. Airgaps as small as 0.1 mm have been used but this adds manufacturing expense to the motor [9].

Miller sites a reasonable airgap length 0.5% of the rotor diameter if the stator length diameter ration, L_{stk}/D_r , is 1 and increasing in proportion to L_{stk}/D_r [8].

5.2.2 Pole arcs

The width of pole arcs present a compromise between smoothness of torque and inductance ratio which relates to the torque density of the machine. Narrower poles result in a higher inductance ratio but a greater torque ripple. Wider pole arcs alleviate torque pulsations but at the expense of efficiency since narrow pole arcs leave more room for windings which will increase machine efficiency. At some point the poles become so narrow that the machine has points of zero torque and thus cannot start from any position. The minimum pole arc is defined by N_r , the number of rotor poles, and m , the number of phases.

$$\min(\beta_s, \beta_r) > \frac{2\pi}{mN_r}$$

Lawrenson defined a “feasible triangle” for SRM pole arcs to help visualize the range of pole arcs with will result in a feasible machine[4]. The Figure 5.1 shows a triangle plotted on axes defined by the stator and rotor pole arcs. It is suggested that $\beta_r \geq \beta_s$ because this allows for a larger slot area without sacrificing aligned inductance. The line XZ is defined by

$$\beta_{s_{min}} = \frac{2\pi}{mN_r}$$

The line YZ is defined by

$$\beta_{r_{min}} = \frac{2\pi}{mN_r}$$

The final line in the triangles is defined by the fact that there should be clearance between the stator and rotor poles in the unaligned position which is represented in the following equation.

$$(\beta_s + \beta_r) \leq \frac{2\pi}{mN_r}$$

The feasible triangle is thus triangle XWZ. Designs along the line XW are usually the most practical but other points can be chosen to achieve specific performance objectives.

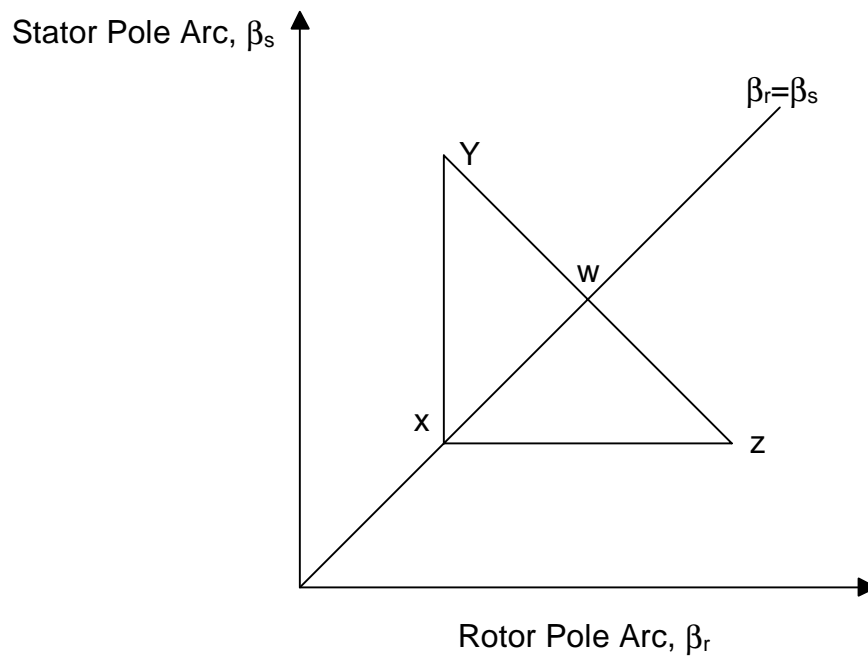


Figure 5.1: Lawrenson feasibility triangle

In terms of the tooth widths, the rotor tooth width should be greater than the stator tooth width by the airgap length, g , or $2g$. In order to ensure a low unaligned inductance

there must be clearance between the rotor and stator teeth. The following equations are used to calculate the pole widths from the pole-arcs.

$$t_s = 2(r_r + g)\sin\frac{\beta_s}{2}$$

$$t_r = 2r_r \sin\frac{\beta_s}{2}$$

5.2.3 Rotor slot depth or rotor tooth length

The tooth must be sufficiently long so that the unaligned inductance is low.

Miller suggest two rules of thumb: 1) the slot depth should be at least 20-30 times the airgap length and 2) $d_r = \frac{t_s}{2}$ [8].

5.2.4 Rotor yoke thickness

The rotor yoke should be thick enough to carry the maximum rotor flux without saturating. From this the rotor yoke should be at least half the rotor tooth thickness and increasing the thickness 20—40% more allows for yoke sections which are common to different phases [8].

The stator yoke is subject to the same magnetic constraints as the rotor yoke. The stator yoke also has mechanical constraints requiring that the designed motor have a stiff stator which will limit stator ovalization and decreases vibration and noise.

5.2.5 Stator slot depth

The stator slot depth has already been defined by all of the previously calculated dimensions. It is desirable to have a large stator slot area to all the maximum area for

windings. A larger area will result in lower copper losses because a larger conductor can be used. The stator slot area can be calculated from

$$d_s = \frac{1}{2}(D_s - D_r - 2(g + y_s))$$

5.2.6 Number of Turns

Miller suggests that the number of turns can be estimated by assuming that at a specified speed the conduction angle of the power transistors has a certain value, Δ , the stroke angle in radians. B_s is the saturation flux density. The equations below show the derivation of an expression for the number of turns per phase if the maximum back emf is equal to the supply voltage. Again the phase resistance is ignored.

$$\psi_{peak} = \frac{V_s \Delta}{\omega}$$

Next the expression for flux linkages is written

$$\psi_{peak} = t_s L_{stk} B_s 2N_p$$

The last two equations are then combined.

$$N_p = \frac{2\pi V_s}{\omega(t_s L_{stk} N_r B_s)m}$$

5.3 Calculation of Losses

Losses calculations were not implemented in the sizing program to calculate efficiency. Instead, efficiencies calculated from experimental data were used in the sizing algorithm. This was due to the complexity of calculating iron losses in the SRM which required detailed knowledge of flux densities at several different points. The computation of copper losses is straightforward but of little value when it cannot be

combined with iron losses to compute machine efficiency. A brief discussion of techniques for calculating losses is presented for the reader's benefit.

5.3.1 Copper Losses

The copper losses of an SRM are simply calculated from the phase resistance; number of phases, m ; and the rms current as is shown in the equation below [4].

$$P_{CU} = m \cdot I_{rms} \cdot R_{ph}$$

The phase resistance can then be calculated based on the average winding length, the cross sectional area of the conductor, the resistivity of copper, and the number of turns.

$$R_{ph} = \rho \frac{Nl_c}{s_a}$$

5.3.2 Iron Losses

Switched reluctance motors have a higher commutation frequency than comparable AC machines. The flux density waveforms also contains many high frequency harmonics because the SRM is not excited with a sine wave. SRMs have a lower iron volume than other AC motors but the SRMs experience high local flux densities. The fact that the flux density waveform is non-sinusoidal prevents the direct use of the Steinmetz's equations. Some work has been done which uses harmonic components and local flux densities to apply the Steinmetz's equations to local regions of the SRM [6, 8, 15]. Figure 5.2 shows the flux densities waveforms in different areas of the SRM.

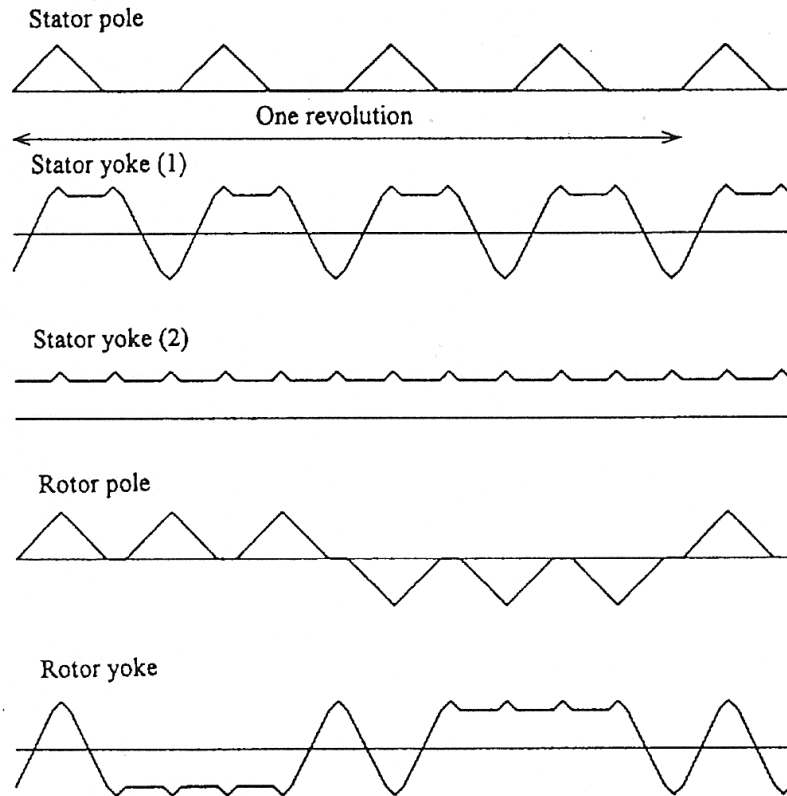


Figure 5.2: Flux waveforms in SRMs

5.4 Reluctance Model Introduction

The importance of the aligned and unaligned inductances of the SRM has been discussed in Chapters 2 and 3. This was a major focus of this thesis work. It is a first step in the sizing equation to determine the constants K_B and K_2 . These cannot be easily obtained for a switched reluctance motor which operates in various states of magnetic saturation. For this reason a reluctance model of the motor was proposed which would include saturation effects.

Simple analogies can be drawn between magnetic and electric quantities. These are shown in the Table 1 below.

Electric		Magnetic	
Quantity	Unit	Quantity	Unit
emf (E)	Volts/meter	mmf (H)	Ampere turns/meter
Potential (V)	Volts	Potential (F)	A turns
Resistance (R)	Ohms	Reluctance (R)	1/henry
Current (I)	Amperes	Flux (Φ)	Weber
Current Density (J)	Amperes/meter ²	Flux Density (B)	Weber/meter ² =Tesla

Table 5.1: Electrical and magnetic analogies

The following equations can be written which are then analogous to Ohm's Law (Ampere's Law).

$$H = \mathfrak{R}\Phi$$

$$B = \mu H$$

The reluctances were calculated following the equation below

$$\mathfrak{R} = \frac{l}{\mu A} = \frac{l}{\mu_o \mu_r A}$$

where l is the flux path length, A is the cross sectional area of the path, μ_o is the permeability of free space, and μ_r is the relative permeability of the flux path.

In the case of the reluctance models H will be known from the current and number of turns and R will be calculated from the machine geometry and steel properties.

This flux, Φ , will then be solved.

$$\Phi = \frac{Ni}{\mathfrak{R}}$$

Once the flux is calculated the flux density can be determined based on the cross sectional area through which a give flux passed.

$$B = \frac{\Phi}{A}$$

The next two equations show several relationships. The most important being the calculation of inductance which was the focus of the reluctance models.

$$\lambda = \Phi N = \frac{N^2 i}{\mathfrak{R}} = Li$$

Here λ is flux linkage in volt seconds and L is inductance in henrys.

$$L = \frac{N^2}{\mathfrak{R}}$$

The complexity of the magnetic circuit over its electrical counterpart was that the reluctance was a non-linear function of flux density. This dependence required iterative calculations to solve the mesh equations. First an unsaturated reluctance was chosen and the flux density calculated. Then this flux density was used to modify the reluctance path. Iteration would continue until the change in reluctance was small.

5.5 Simple Reluctance Model

A very simple model of the SRM was created using only two parallel flux paths. This model obviously assumed that no fringing of flux lines occurred in the air gap and that there were no leakage paths. The magnetic circuit is shown in figure 5.3.

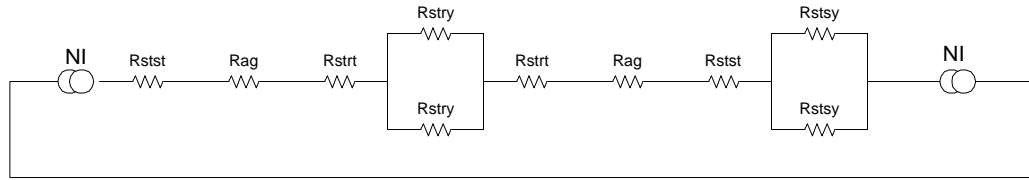


Figure 5.3: Simple Reluctance Model

The simple model discussed above was unsuitable for any rotor positions other than aligned and was inaccurate at high currents where the steel saturated in the aligned position. It is now believed that this was primarily due to the iterative technique used. In an effort to determine the unaligned inductance, a more complex model was designed based on [7].

5.6 Detailed Reluctance Model

This model divided the motor geometry into a desired number of flux paths all of the same width. The divided geometry at several rotor positions and related circuit model are shown in Figures 5.4 and 5.5 respectively.

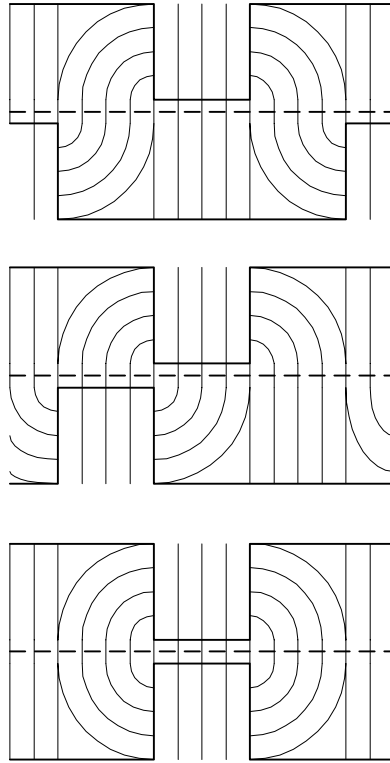


Figure 5.4 Flux paths for the detailed reluctance model

Originally quarter circle arcs were assumed for the fringing flux but this was inaccurate because the actual motor was curved. A better approximation was eighth circle arcs on the rotor side and quarter circle arcs on the stator side.

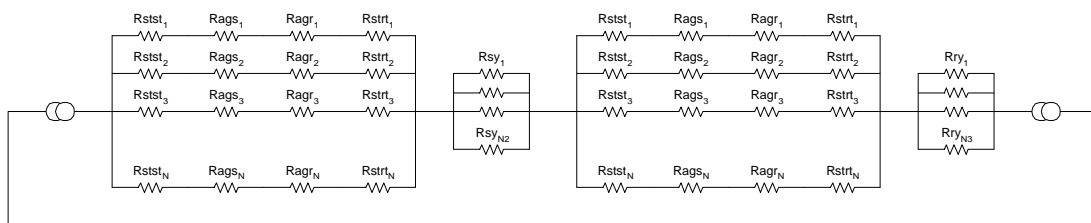


Figure 5.5: Detailed reluctance model

The following equations were solved to calculate the flux in each path

$$H_{ag} = 2Ni \frac{R_{ageq_1}}{2R_{ageq_1} + R_{ryeq_1} + R_{syeq_1}}$$

$$R_{ag1} = R_{strt_1} + R_{agr_1} + R_{ags_1} + R_{stst_1}$$

$$R_{ag2} = R_{strt_2} + R_{agr_2} + R_{ags_2} + R_{stst_2}$$

$$R_{agN} = R_{strt_N} + R_{agr_N} + R_{ags_N} + R_{stst_N}$$

$$\begin{bmatrix} H_{ag} \\ H_{ag} \\ \vdots \\ H_{ag} \end{bmatrix} = \begin{bmatrix} R_{ag1} & 0 & \cdots & 0 \\ 0 & R_{ag2} & 0 & \vdots \\ \vdots & 0 & \ddots & 0 \\ 0 & \cdots & 0 & R_{agN} \end{bmatrix} \begin{bmatrix} \Phi_1 \\ \Phi_2 \\ \vdots \\ \Phi_N \end{bmatrix}$$

Reluctances with the suffix “eq” were the equivalent resistances for a block of resistors. In order to solve the system for different rotor positions, the rotor side air gap and steel reluctances were shifted down and the last reluctances moved to the top of the block.

The permeability in the steel was assumed maximum for the first iteration. The flux density of each tube was then calculated in the steel sections and the flux density was used to select a new permeability from a look-up table containing the steel’s BH curve data. This would be continued until the permeability converged to a value. If only the look-up table were used the permeability would never converge. Initially the flux density will be very low which will lead to the steel being set to maximum permeability for the next iteration. The high permeability will lead to a high flux density which will cause the permeability to be set low again. The program would continue “bouncing” between these extremes.

This problem was corrected by adding a low proportional constant which acted on the difference in look-up table permeability between the prior and present iteration. This term was then added to the past permeability causing it to slowly reach a steady state

value. Proportional control led to another complication in the form of a steady state error – the final flux densities did not correspond to the proper permeabilities. The addition of an integral term was required and the results were improved. It was also found that adding more points to the BH look-up table improved the speed of convergence.

Originally, the cost function was the last error in the sum of the norms of the permeability matrices. The accepted change, delta, must be significantly less than the proportional constant otherwise a small change (small error) will be achieved before convergence is achieved. This could also lead to permeability values which do not match flux density values. The cost function was changed to the sum of permeability errors for all flux tubes and this corrected the problem. Figure 5.6 shows a flowchart for the flux tube inductance calculations.

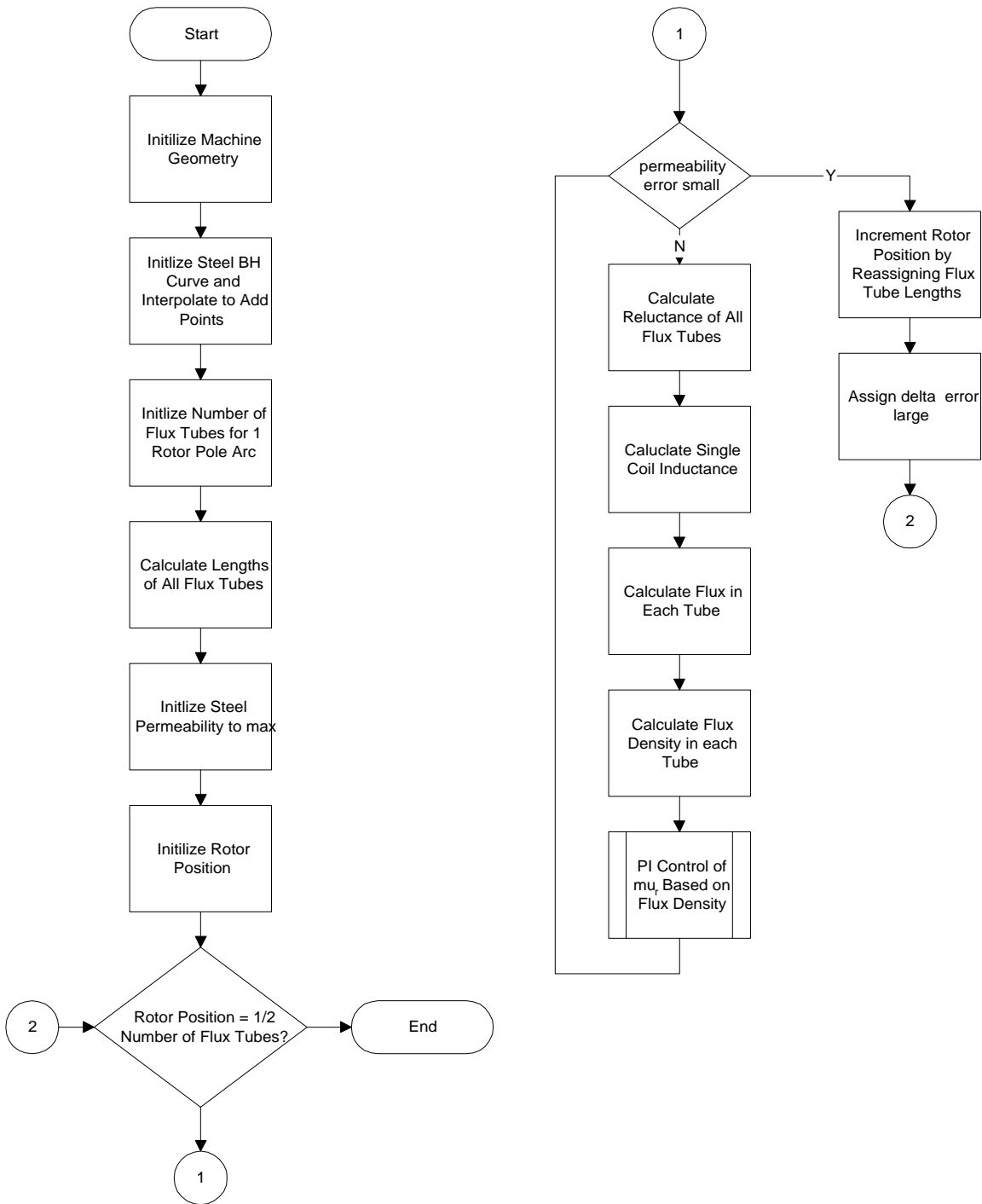


Figure 5.6: Reluctance program flow chart

5.7 Corda and Stephenson Unaligned Inductance Model

Corda and Stephenson developed a geometrically detailed reluctance model for a switched reluctance machine in the unaligned positions. These equations assume no saturation in the steel since the airgap is large. The flux path lengths shown in Figure 5.7 are calculated and permeabilities of five different regions shown in Figure 5.8 are calculated. These are then used in the following equation to calculate the total unaligned inductance [1].

$$\begin{aligned}L_o &= \frac{4}{i}(\psi_1 + \psi_3 + \psi_4 + \psi_5 + \psi_6) \\ &= 4(L_1 + L_3 + L_4 + L_5 + L_6) \\ &= N^2 \mu_o l(P_1 + P_3 + P_4 + P_5 + P_6)\end{aligned}$$

All equations presented in [1] were entered written in a MATLAB script and the accuracy of the technique was compared to experimental data for an SRM.

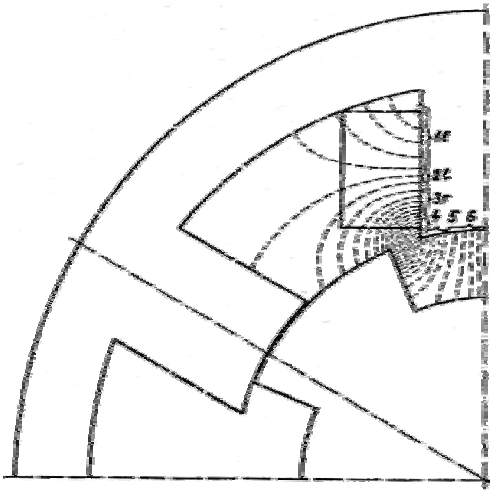


Figure 5.7: Flux paths for Corda and Stephenson model

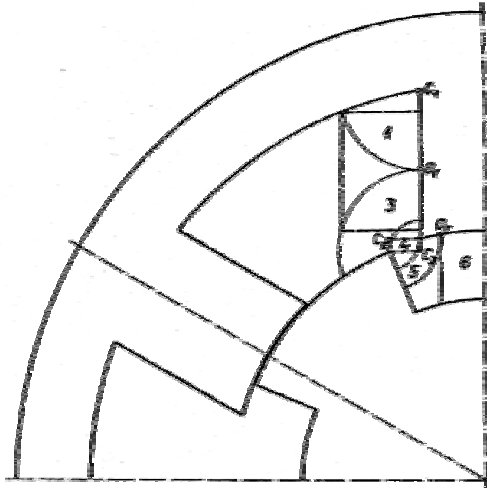


Figure 5.8: Permeability regions for Corda and Stephenson model

5.8 Radun Analytical Inductance Calculations

Many sizing schemes require finite element modeling to determine inductance ratios and flux densities or rely on empirical parameters based on physical machines. These approaches do not provide the insight into design and sizing that closed form equations allow. Some work has been done by Radun in [10, 11, 12] to develop closed form solutions for inductance and flux linkage. The sizing equations based on this technique are presented below. These equations are based on electromagnetic field and boundary conditions. This technique could be compared to finite element model with only one element. Figure 5.9 shows the machine geometry used and the field applied. The analysis of considering step nature of the field using a Fourier series results in the summation of the following unaligned inductance equations.

$$L_u = 8\mu_o N^2 l_{stk} l \sum_{n_{odd}} \frac{\frac{\sin\left[\frac{n\pi l_1}{l}\right]}{l_1} + \frac{\sin\left[\frac{n\pi l_2}{l}\right]}{l_2}}{(\pi n)^2 \tanh\left[\frac{n\pi h}{l}\right]}$$

This equation is applied in a MATLAB script included in Appendix D.

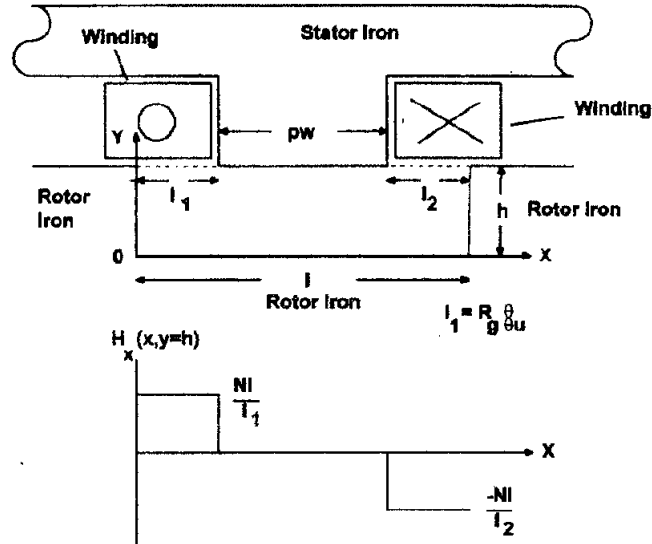


Figure 5.9: Radun inductance model

5.9 Simple Aligned Inductance Model

Because of the difficulty in applying the detailed reluctance model or a technique from literature to calculating the aligned inductance a very simple model was developed. This model assumes no saturation in the rotor and stator yoke and no fringing flux in the airgap. These are reasonable assumptions according to [13]. There is now only one flux path through the rotor and stator teeth and both sides of the airgap. The stator and rotor

teeth are assumed the same width which is true in most designs. This reluctance model now only has 3 different elements: 2 stator teeth, 2 rotor teeth, and 2 airgap lengths. The model is also simplified because the rotor and stator teeth will see the same flux density. This make iterative computation of the flux densities and permeabilities simpler. Figure 5.10 shows the aligned cross section of the SRM and its associated magnetic equivalent circuit.

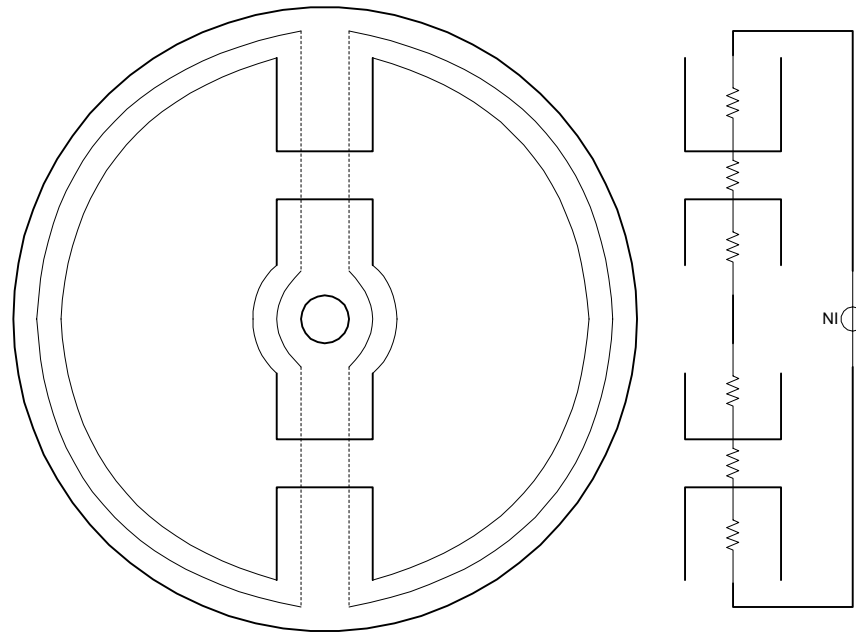


Figure 5.10: Aligned inductance model

A different technique was used for iteratively computing the permeability. From the BH curve, quasi-linear relative permeability vs. flux density equations were written. If the calculated flux density was in the nonlinear region a bisection technique was used. This equation allowed a much more rapid and accurate convergence than the proportional

integral technique described earlier. Figure 5.11 shows points labeled 1 through 4 in saturation region of the curve. This illustrates how the program converges to the actual permeability based on the flux density calculated from the permeability used in the last iteration. The application of these technique can be seen in Appendix C.

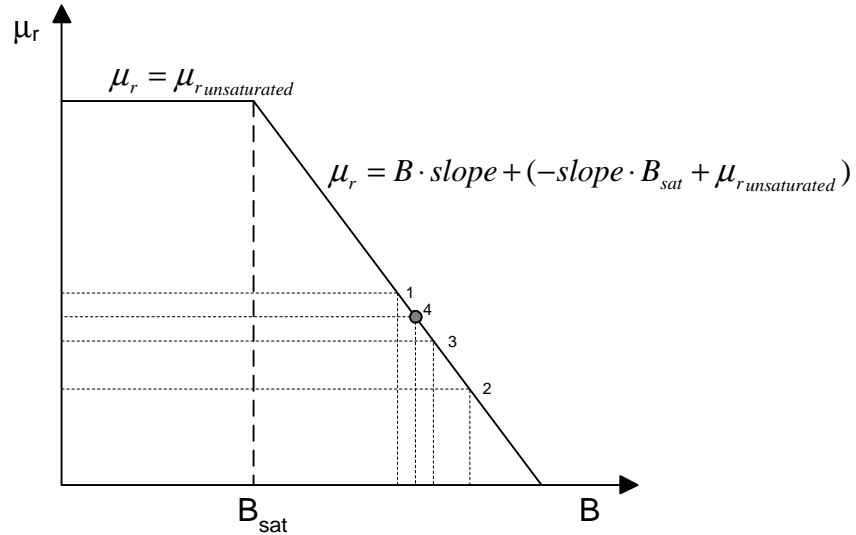


Figure 5.11: Permeability vs. flux density plot and bisection technique

5.10 Phase and Coil Inductances

Special attention will be brought to the mutual inductance between adjacent coils in a phase as this was a point of confusion early in the research. The mutual inductances of the coils were not considered initially. This resulted in a factor of four difference in the overall inductance. Figure 5.12 shows the inductances.

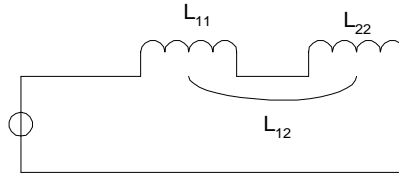


Figure 5.12: Schematic of one phase with series coils

The flux linkage between coil L_{11} and L_{22} will be the same in both directions resulting in the equation below.

$$L_{global} = L_{11} + L_{22} + 2L_{12}$$

If the flux linkage between coils is equal to the self-linkage then the following equation will be true.

$$L_{global} = \frac{N_1^2}{R} + \frac{N_2^2}{R} + \frac{N_1 N_2}{R} = \frac{(2N)^2}{R}$$

Chapter 6

Results

6.1 Introduction

This chapter discusses the results of the various techniques used to calculate the aligned and unaligned inductances. It also discusses the results of the sizing program.

6.2 Unaligned Inductance Results

Figure 6.1 shows the unaligned inductance for each of the different modeling techniques. Figure 6.2 shows the error of each of these techniques compared to the experimental results. As would be expected, the commercial FEA package produced the most accurate results; however the error was nearly 20%. The flux tube technique and the technique described in [12] both resulted in nearly 60% error and the technique from [1] had over 30% error. No technique was particularly accurate, but all besides the FEA, were computed quickly enough that they could be used in the sizing program. Also, without other machines for comparison it is not known how accurate these techniques are for various size machines.

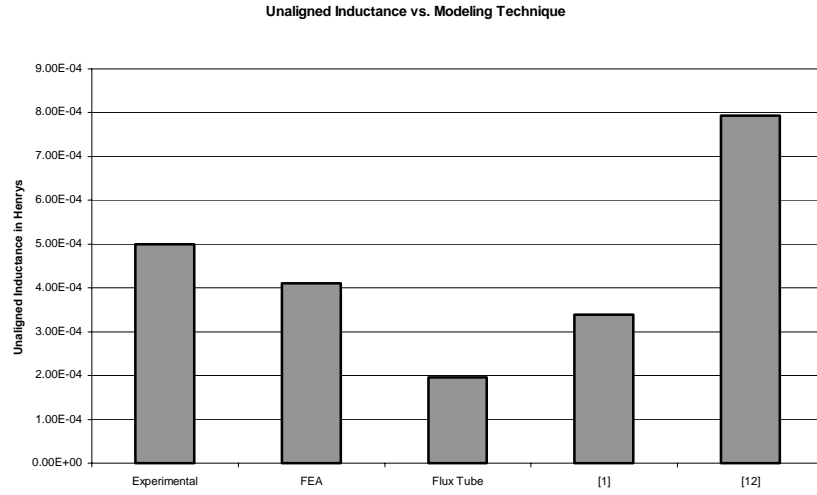


Figure 6.1: Comparison of unaligned inductance calculations for several methods

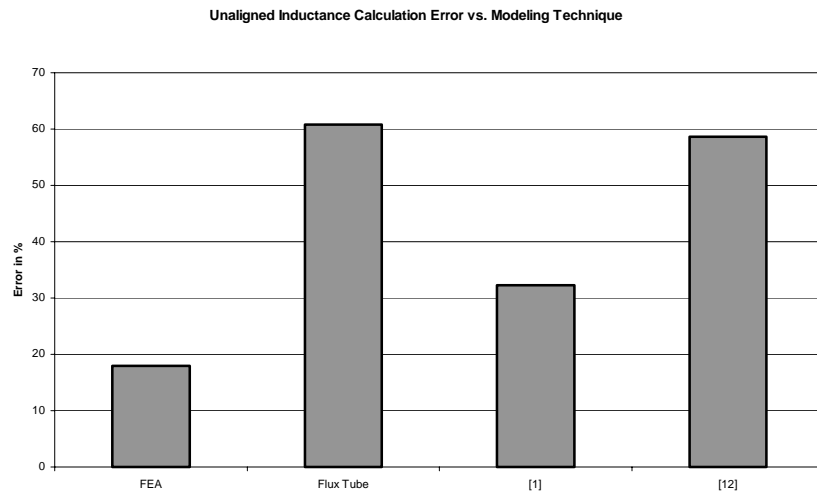


Figure 6.2: Percent errors for unaligned inductance calculations

6.3 Detailed Reluctance Model Results

Figures 6.3-5 show the results of the detailed reluctance model. With this model it was possible to calculate the flux density across the entire airgap. These figures show the rotor tooth flux density at the bottom of the plot and the stator tooth flux density at the top of the plot. Figure 6.3 shows the rotor in the unaligned position with half of the rotor tooth on the left and half on the right. This shows reasonable flux density values based on finite element results. Note that the stator pole is at the top, center of the figure and that half of two rotor poles are on either side of the graph at the bottom. The progression of Figures 6.3-5 shows the rotor moving clockwise or to the right.

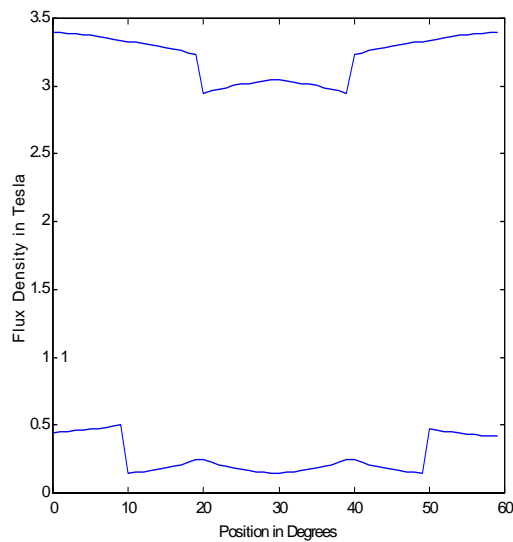


Figure 6.3: Pole flux densities for the unaligned position

Figure 6.4 shows the tooth edges becoming aligned. The flux density was greatest at this edge. Again this is an expected result.

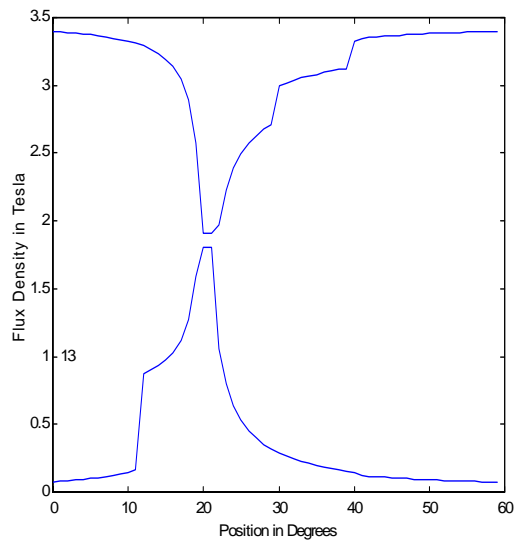


Figure 6.4: Pole flux densities for a partially aligned position

Figure 6.5 shows the aligned rotor position. Both rotor and stator teeth have a peak flux density of approximately 1.6 T which concurred with finite element results. The steps which occur at the midpoints of the teeth were due to a modeling assumption: all flux entering the sides of a pole was averaged over half of the pole on the side that the flux entered.

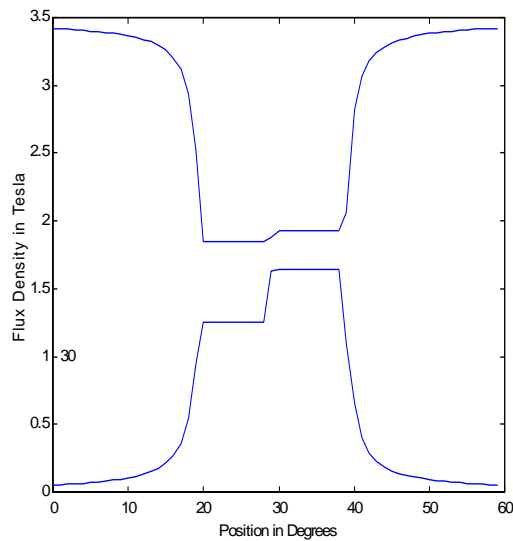


Figure 6.5: Pole flux densities for the aligned position

Despite the fact that the detailed reluctance model generated flux density values that were quite reasonable, the calculated inductances shown as solid lines in Figure 6.6 below were substantially lower than the FEA values plotted as dashed lines. It should be noted that the shape of the inductance profile with changing rotor position and current were as expected but the magnitude was in error. It is possible that with machines of different sizes to compare, a scaling factor could be developed.

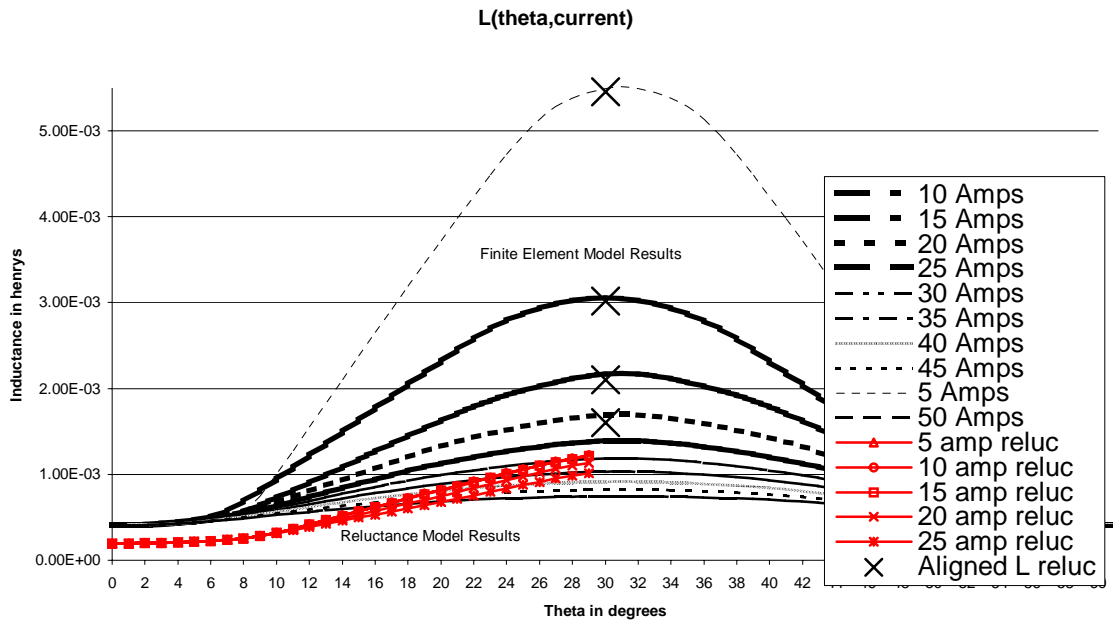


Figure 6.6: Calculated inductances from FEA and the reluctance models

6.4 Aligned Inductance Model

Figure 6.6, above, also shows the result of the simple aligned inductance model. The results are plotted as **X**s above the aligned position of 30°. This shows that errors ranging from 4-10% were achieved for different currents. These results indicate that a very simple model is sufficient for calculating both saturated and unsaturated aligned inductance.

6.5 Sizing Program Verification

Figure 6.7 shows the result of the sizing program when speed was calculated from all known machine dimensions and from the measured torque, current, and efficiency.

Figure 6.8 shows the result of the sizing program when efficiency was calculated from all known machine dimensions and from measured speed, torque, and current. It can be seen that the sizing program produced results which varied from the measured parameters by – 33% to 20%. These may or may not be acceptable results for a designer. Given the errors present in all methods of calculating inductances the error of the overall sizing program seems relatively low for this verification study.

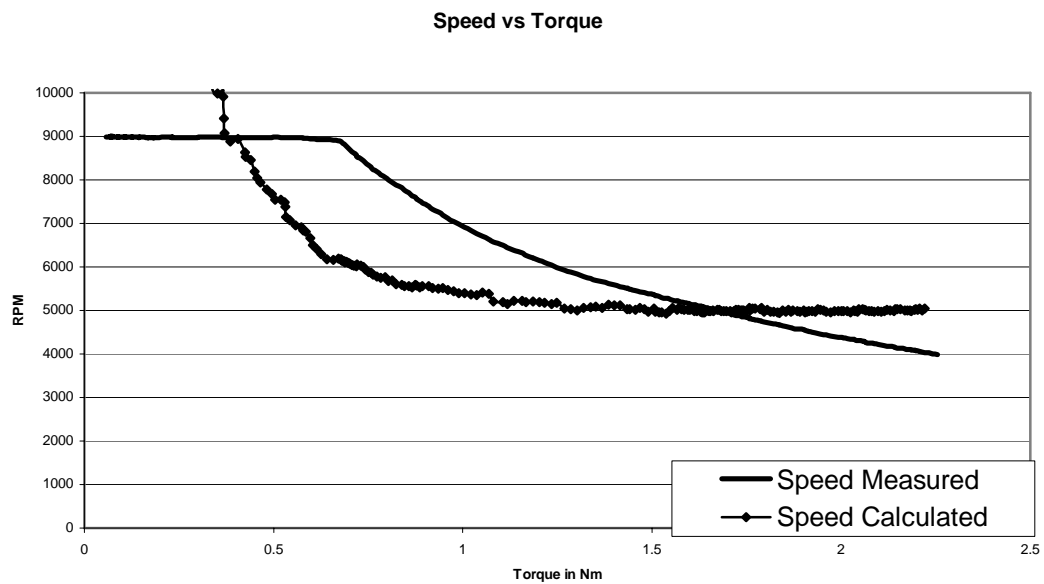


Figure 6.7: Speed calculated from sizing equation compared to experimental data

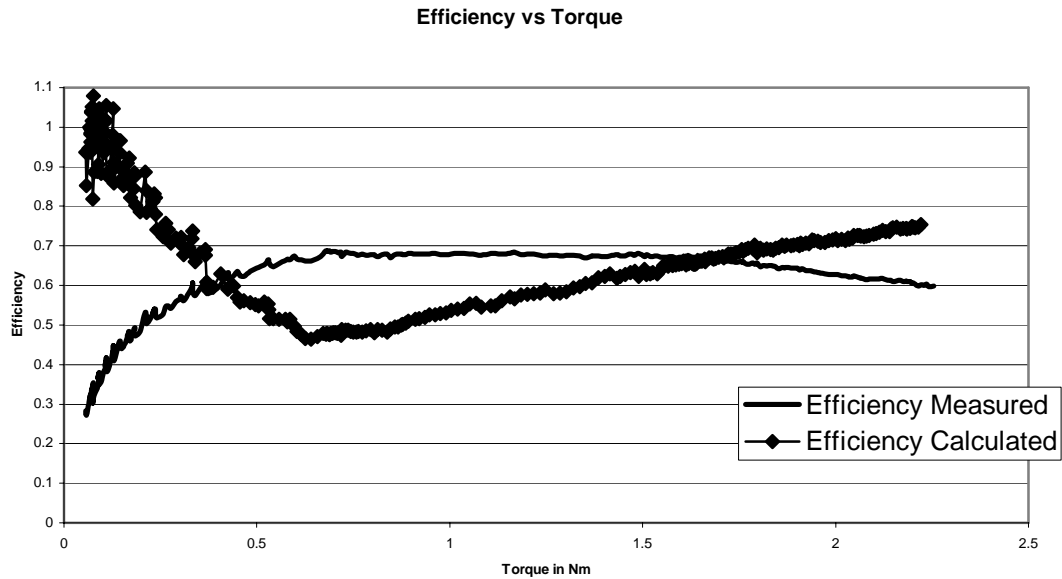


Figure 6.8: Efficiency calculated from sizing equation compared to experimental data

6.6 Sizing Program Dimensions

Aware of the limitations of the sizing program, machine specifications were entered and machine dimensions were generated at 3 different points on the speed torque curve. Because a losses model was never created efficiencies from experimental data were used in the sizing program. For the sizing program to be truly useful a losses model will need to be added. As was described in Chapter 4, after an initial calculation of dimensions the sizing program calculates the torque to verify that it matches specified value. The tables below show that often the final calculated torque exceeds the specified value but it can also be seen that the designed length, L , was significantly longer than that of the actual machine. From an understanding of the sizing equation it is known that the

torque will be linearly dependent on the length so the designer can choose to shorten the rotor. Even with modification the length calculated by the sizing program will be much greater than that of the actual machine. The reason for this is not understood especially in light of the lower error achieved from the sizing program in the verification study. Another large discrepancy is seen in the number of turns, N. This is because ampere turns, NI, are the important factor. The current could be lowered by increasing the number of turns.

	Actual Motor	Case 1	Case 2	Case 3
RPM		4000	9000	9000
T		2.25	0.5	0.1
eta		0.7	0.7	0.35
T(calc)		3.542	0.7871	0.15742
Ns	8	8	8	8
Nr	5	6	6	6
Sod	0.0776	0.0776	0.0776	0.0776
L	0.04	0.48294	0.10732	0.042928
D	0.0349	0.0388	0.0388	0.0388
g	0.0001	0.0001	0.0001	0.0001
hr	0.00745	0.003785	0.003785	0.003785
br	0.00668	0.00757	0.00757	0.00757
hcr	0.004	0.005299	0.005299	0.005299
hs	0.01255	0.011976	0.011976	0.011976
bs	0.00668	0.007609	0.007609	0.007609
hc	0.0088	0.007424	0.007424	0.007424
N	60	5.443	10.886	27.215
I		37.352	18.676	7.4703
Lu	0.0005	9.01E-05	8.01E-05	0.0002
Las		0.003883	0.003452	0.008629
Bs		1.8131	1.8131	1.8131

Table 6.1: Sizing equation output comparison

Chapter 7

Conclusion

7.1 Conclusion

This research has investigated automotive electrical systems and discussed the need for and requirements of electromechanical actuation and propulsion in modern automotive vehicles. The low cost, easy assembly, and low rotor inertia of the SRM make it well suited for many automotive applications. One of the drawbacks of SRMs for the automotive industry is the time to market due to the SRMs nonlinear magnetic operation. This research sought to provide a “first pass” design tool for SRM designers. A D^2L sizing equation was developed for SRMs and was programmed in a MATLAB script. Beyond sizing, the MATLAB script also included design guidelines which provide the designer with a complete set of dimensions to model the machine in a more accurate but much more time intensive finite element analysis (FEA) program. The MATLAB script also gives the designer the ability to modify the calculated dimensions and view their effect on output torque.

In developing the sizing program, a large portion of this research was spent investigating maximum and minimum inductance calculations for the SRM. The

inductance ratio constant, K_2 , is an important element in the sizing program and cannot be easily determined without some analysis. Three methods for calculating the unaligned inductance were investigated [1, 10, 12, 13]. These methods were implemented and their results compared to experimental and FEA results. None were shown to produce results closer than 18% for the motor used in this research. Three methods were implemented to calculate the aligned inductance [12, 13]. Two of these were relatively complex and ultimately never produced accurate results. In an effort to understand the problem a third very simple model was created and shown to calculate the aligned inductance with a 4-10% error.

The completed sizing program was verified using speed, torque, current, and efficiency data collected from the studied motor, a 42 V motor capable of providing 2.5 Nm at 4000 rpm. Over the full range of torque, the error between both calculated and measured efficiency and between the calculated speed and measured speed varied from -33% to 20%. This may be an acceptable starting point in some but not all situations. The sizing program was then used to generate a complete geometry for 3 given points on the SRMs speed torque curve. These results showed considerable variation from the designed machine at higher torques and the reason for this remains to be determined.

7.2 Future Work

Future work could be directed towards applying the sizing program to a wider variety of machine sizes which would allow for its greatest areas of inaccuracy to be determined. More work could also be directed at a determination of aligned, unaligned inductances, and flux linkages. An accurate model of inductances over the full stroke

angle of the machine would allow electrical modeling and very accurate torque calculations without the use of an FEA program. Finally, This research did not implement a calculation of η , efficiency, in the sizing program. Instead, efficiency values obtained from test data were used. To be truly useful the sizing program must be able to calculate the iron and copper losses of a given machine at specified load conditions. Literature in this area was investigated and commented on but it was not implemented in the sizing program.

APPENDIX A

MATLAB Code for Verification of the Sizing Script

```
%%%%%%%%%%%%%%%%%%%%%%%%%%%%%%%%%%%%%%%%%%%%%%%%%%%%%%%%%%%%%%%%%%%%%%%%%
%Paul Gemin
%SRM Sizing Program to verify sizing equation
%This program estimates the size and internal dimensions
%of a machine to meet desired specifications
%%%%%%%%%%%%%%%%%%%%%%%%%%%%%%%%%%%%%%%%%%%%%%%%%%%%%%%%%%%%%%%%%%%%%%%%%

clear all

%ELECTIRCAL PROPERTIES
N=60 %Number of turns per phase
m=3; %Number of phases

%GEOMETRY
Ns=8; %Number of Stator Poles
Nr=6; %Number of Rotor Poles

Rod=.0349; %Rotor Outer Diameter
Rth=.00745; %Rotor Tooth Height
Rtw=.00668; %Rotor Tooth Width
Ryt=.004; %Rotor Yoke Thickness
lag=.0005; %Length of Airgap
Sod=.0776; %Stator Outer Diameter
Sth=.01255; %Stator Tooth Height
Stw=0.00668; %Stator Tooth Width 0.0276
Syt=.0088; %Stator Yoke Thickness
L=.040; %Machine Length

%STEEL PROPERTIES
%Quasi-linear steel BH curve
mur_unsat=8300; %unsaturated steel relative permeability
slope=-7518; %slope in saturation region mur v. B graph
Bsat=1; %beginning of saturation region

%LOAD DATA FILE
SRMfile %load speed, Torque, Current, and Efficiency data
RPM=SRM_data([1:88 90:300],1);
T=SRM_data([1:88 90:300] ,2);
I=SRM_data([1:88 90:300],3);
```

```

eta=SRM_data([1:88 90:300],4);
w=RPM.*(2.*pi./60);
P=w.*T;

%AMPERE LOADING
I=I./sqrt(m);
theta_c=2*pi/(Nr*2);
%theta_c=Stw/(pi*2*Rod)*2*pi;%conduction angle
Q=2.*N.*I./(pi.*Rod);%Ampere loading (check N or 2N)
Kd=m*theta_c*Nr/(2*pi);

%INDUCTANCE PROPOERTIES FROM INDUCTANCE PROGRAM
Lmin=.0005;%unaligned inductance
for k=1:1:length(I)

L_input=[Ns,Nr,L,Sod,Rod,lag,Rth,Sth,Stw,Rtw,N,I(k),Bsat,mur_unsat,slop
e];
[Las Btemp]=L_aligned(L_input);
Lrec(k)=Las;
K2(k)=1-Lmin/Las;
Bs(k)=Btemp;
end
K2=K2';
Bs=Bs';

%SIZING EQUATION CALCULATIONS
eta_calc=T./(Kd.*K2.*Bs.*Q.*(pi/4).*L.*Rod^2);
w_calc=P./(Kd.*K2.*Bs.*eta.*Q.*(pi/4).*L.*Rod^2);
RPM_calc=w_calc.*(60./(2*pi));

```

APPENDIX B

MATLAB Code for the First Pass Sizing Script

```
%%%%%%%%%%%%%%%%%%%%%%%%%%%%%%%%%%%%%%%%%%%%%%%%%%%%%%%%%%%%%%%%%%%%%%%%%
%Paul Gemin
%SRM Sizing Program
%This program estimates the size and internal dimensions
%of a machine to meet desired specifications
%%%%%%%%%%%%%%%%%%%%%%%%%%%%%%%%%%%%%%%%%%%%%%%%%%%%%%%%%%%%%%%%%%%%%%%%%

clear all
%%%%%%%%%%%%%%%%%%%%%%%%%%%%%%%%%%%%%%%%%%%%%%%%%%%%%%%%%%%%%%%%%%%%%%%%%
%USER INPUTS
%%%%%%%%%%%%%%%%%%%%%%%%%%%%%%%%%%%%%%%%%%%%%%%%%%%%%%%%%%%%%%%%%%%%%%%%%
%ELECTIRCAL PROPERTIES
V=36; %bus voltage
m=3; %Number of phases

%WINDING PROPERTIES
J=3.8754e6; %current densityJ~3.8754e6 A/m^2 for totally enclosed,
           %1.0076e7 A/m^2 for appliance
ksf=.35; %slot fill factor (~0.35-0.5)

%STEEL PROPERTIES
%Quasi-linear steel BH curve
mur_unsat=8300; %unsaturated steel relative permeability
slope=-7518; %slope in saturation region mur v. B graph
Bsat=1; %beginning of saturation region

%GEOMETRY
Ns=8; %Number of Stator Poles
Nr=6; %Number of Rotor Poles

%ESTIMATED EFFICIENCY
eta=.65;

%SIZE CONSTRAINT
Sod=.0776; %maximum stator outside diameter

%DESIRED PERFORMANCE
T=2; %rated torque in Nm
RPM=7000; %rated speed in rpm
```

```

w=RPM*(2*pi/60); %rated speed in rad/sec

%%%%%%%%%%%%%%%%%%%%%%%%%%%%%%%%%%%%%%%%%%%%%%%%%%%%%%%%%%%%%%%%%%%%%%%%
%CALCULATING FIRST PASS CONSTANTS
%%%%%%%%%%%%%%%%%%%%%%%%%%%%%%%%%%%%%%%%%%%%%%%%%%%%%%%%%%%%%%%%%%%%%%%%
%AIRGAP DIAMETER
Dratio=0.5; %ratio of rotor diameter / stator diameter (~0.4-0.7)
D=Dratio*Sod; %Rotor outside diameter

%INDUCTANCE CONSTANT
K2=0.9; % (~0.65-0.9)

%DUTY CYCLE CONSTANT
theta_c=pi/Nr; %conduction angle approximated as the rotor pole arc
Kd=m*theta_c*Nr/(2*pi);

%MAGNETIC LOADING CONSTANT
Bs=1.5; %flux density in stator tooth in aligned position

%POLE WIDTHS
thetap=2*pi/(Ns*2);
bs=D/2*sin(thetap); %stator tooth width
br=D*sin(thetap/2);

%TOOTH HEIGHTS AND YOKE THICKNESSES
hc=bs*1; %height of stator yoke (constant ~0.6-1.2)
hs=(Sod-2*hc-D)/2; %height of the stator pole
hr=br/2; %guideline for selecting rotor tooth height
hcr=br/2*(1.4); %guideline for selecting rotor yoke thickness

%AMPERE LOADING CONSTANT
s=1/Ns*((pi/4)*(Sod-2*hc)^2-(pi/4)*D^2)-hs*bs; %slot cross-sectional
area
NI=s*ksf*J; %ampere turns per phase
Q=2*NI/(pi*D); %Ampere loading constant

%MACHINE LENGTH
L=T/(Kd*K2*eta*Bs*Q*(pi/4)*D^2);

%%%%%%%%%%%%%%%%%%%%%%%%%%%%%%%%%%%%%%%%%%%%%%%%%%%%%%%%%%%%%%%%%%%%%%%%
%CALCULATING SECOND PASS GEOMETRY AND TORQUE
%%%%%%%%%%%%%%%%%%%%%%%%%%%%%%%%%%%%%%%%%%%%%%%%%%%%%%%%%%%%%%%%%%%%%%%%

%AIRGAP DIMENSIONS
%if L/D<=1
% g=D*.005; %airgap 0.5% of rotor diameter
%else
% g=D*L/D*(.005); %longer rotors require a larger airgap for
machining
%end

%if g<0.0001
% g=.0001; %the airgap should not be less than 0.1 mm
%end

```

```

g=.0001

%POLE WIDTHS
thetap=2*pi/(Ns*2);
bs=(D+g*2)*sin(thetap/2); %stator tooth width
br=D*sin(thetap/2);

%NUMBER OF TURNS
N=2*V*pi/(w*m*bs*L*Nr*Bs); %Estimate the number of turns per phase
I=NI/N; %peak phase current

%ALIGNED AND UNALIGNED INDUCTANCE SCRIPTS
Lu=L_unaligned(Ns,Nr,L,D,g,hr,hs,bs,N);
L_input=[Ns,Nr,L,Sod,D,g,hr,hs,bs,br,N,I,Bsat,mur_unsat,slope];
[Las Bs]=L_aligned(L_input);
K2=1-Lu/Las;

%VERIFY TORQUE WITH GIVEN DIMENSIONS
T=L*(Kd*K2*eta*Bs*Q*(pi/4)*D^2)

%OUTPUT ALL DESIGN DATA
Output_data=[Ns;
Nr;
Sod;
L;
D;
g;
hr;
br;
hcr;
hs;
bs;
hc;
N;
I;
Lu;
Las;
Bs]

```

APPENDIX C

MATLAB Code to Calculate Aligned Inductances

```
function [Las, Bs] = L_aligned(L_input)
%%%%%%%%%%%%%%%%%%%%%%%%%%%%%%%%%%%%%%%%%%%%%%%%%%%%%%%%%%%%%%%%%%%%%%%%
%Paul Gemin
%SRM Reluctance Model
%This Program calculates the inductance of 1 phase
%when the rotor is in the aligned position
%it assumes only two flux paths and no fringing
%%%%%%%%%%%%%%%%%%%%%%%%%%%%%%%%%%%%%%%%%%%%%%%%%%%%%%%%%%%%%%%%%%%%%%%%
Ns=L_input(1);
Nr=L_input(2);
L=L_input(3);
Sod=L_input(4);
D=L_input(5);
g=L_input(6);
hr=L_input(7);
hs=L_input(8);
bs=L_input(9);
br=L_input(10);
N=L_input(11);
I=L_input(12);
Bsat=L_input(13);
mur_unsat=L_input(14);
slope=L_input(15);

%GEOMETRY
Rod=D;    %Rotor Outer Diameter
Rth=hr;   %Rotor Tooth Height
Rtw=br;   %Rotor Tooth Width
Lag=g;    %Length of Airgap
Sth=hs;   %Stator Tooth Height
Stw=bs;   %Stator Tooth Width

%MATERIAL PROPERTIES
muo=(4*pi)*10^(-7);    %permeability of freespace
%Quasi-linear steel BH curve
mur=mur_unsat;        %unsaturated steel permeability
slope=-7518;          %slope in saturation region mur v. B graph
Bsat=1;               %beginning of saturation region
```

```

%PATH LENGTHS
Lstst=Sth; %length of stator tooth flux path
Lstrt=Rth; %length of rotor tooth flux path

H=N*I;
Bmid=0;
k=1;
err_total=1e6;
while abs(err_total)>100
    Rstst=Lstst/(mur*muo*Stw*L);
    Rag=Lag/(muo*Stw*L);
    Rstrt=Lstrt/(mur*muo*Rtw*L);

    Rtotal=2*Rstst+2*Rag+2*Rstrt;
    phi=inv(Rtotal)*H;

    B=phi/(Stw*L);
    %%%%%%%%%%%%%%%%%%%%%%%%%%%%%%%%%%%%%%%%%%%%%%%%%%%%%%%%%%%%%%%%%%%%%%%%%
    %REASSIGN RELATIVE PERMEABILITIES
    %%%%%%%%%%%%%%%%%%%%%%%%%%%%%%%%%%%%%%%%%%%%%%%%%%%%%%%%%%%%%%%%%%%%%%%%%
    if B>Bsat
        if B>(Bsat+Bmid)
            Bmid=Bmid+(2.1-Bsat)/(2^k);
            mur=slope*(Bsat+Bmid)+(-slope+mur_unsat);
        elseif B<(Bsat+Bmid)
            Bmid=Bmid-(2.1-Bsat)/(2^k);
            mur=slope*(Bsat+Bmid)+(-slope+mur_unsat);
        end
        err_total=abs(mur-(slope*(B)+(-slope+mur_unsat)));
    else
        err_total=abs(mur-mur_unsat);
    end
    k=k+1;
end
Lcoil=(N^2)/Rtotal; %coil inductance

%phase inductance is 4*Lcoil
Las=Lcoil*4; %Phase inductance
Bs=B; %flux density in the tooth

```

APPENDIX D

MATLAB Code for Calculating Unaligned Inductances

```
function [Lu] = L_unaligned(Ns,Nr,L,D,g,hr,hs,bs,N)
%%%%%%%%%%%%%%%%%%%%%%%%%%%%%%%%%%%%%%%%%%%%%%%%%%%%%%%%%%%%%%%%%%%%%%%%
%L_unaligned calculates the minimum unaligned inductance using
%equations developed by A. Radun
%
%%%%%%%%%%%%%%%%%%%%%%%%%%%%%%%%%%%%%%%%%%%%%%%%%%%%%%%%%%%%%%%%%%%%%%%%

muo=(4*pi)*10^(-7);

lstk=L;%rotor length
Rg=D/2;%rotor outside radius
Rsy=D/2+hs;%inside radius of stator yoke
Rry=D/2-hr;%outside radius of rotor yoke
tw=bs;%tooth width
thetar= 2*pi/Nr;%angular spacing between the rotor pole centers
thetap=tw/(pi*2*Rg)*2*pi;%angular extent of the poles
thetas=2*pi/Ns;%angular spacing between the stator poles

lr=Rg*(thetar-thetap)+2*g;%length of rotor "slot"
hr=Rg-Rry;%
lr1=(pi*2*Rg/Nr-2*tw)/2;%spacing between left side of rtooth and
    %right side of stooth
lr2=lr1;%spacing between right side of rtooth and left side of
    %stooth
ls1=lr1;
hs=Rsy-Rg;%
lw=Rg*(thetas-thetap)/2;%
ls=Rg+Rsy/2*(thetas-thetap)+2*g;%
csx=0;
for n=1:1:40
    csx=-muo*ls/(pi*n)^2*(sin(pi*n*lw/ls))^2+csx;
end
csy=-muo*lw/2*ls;

%Calculate Rotor Contribution to the Unaligned Inductance
sumr=0;
for n=1:2:41
```

```

nextr=(sin(pi*n*lr1/lr)/lr1+sin(pi*n*lr2/lr)/lr)/((pi*n)^2*tanh(pi*n*hr
/lr));
    sumr=sumr+nextr;
end
Lur=4*muo*N^2*lstk*lr*sumr;

%Calculate Stator Contribution to the Unaligned Inductance
sums=0;
for n=1:1:40
    asp=muo*ls^2/(2*(pi*n)^3)*sin(pi*n*lw/ls);

ash=2*muo*lw*hs*ls*sin(pi*n*ls1/ls)/((pi*n)^2*ls1*sinh(pi*n*hs/ls));
    nexts=ash*(cosh(pi*n*hs/ls)-
ls^2/((pi*n)^2*hs*ls)*sinh(pi*n*hs/ls)*sin(pi*n*lw/ls))...
    +asp*(cos(pi*n*lw/ls)-ls/(lw*pi*n)*sin(pi*n*lw/ls));
    sums=sums+nexts;
end
Lus=2*N^2*lstk/(hs*lw)*(2/3*csy*hs^2-csx*lw/2+sums);

Lu=Lur+Lus;

```

BIBLIOGRAPHY

- [1] Corda, J., J. M. Stephenson. "Analytical Estimation of the Minimum and Maximum Inductances of a Double-Salient Motor." *Proceedings of the International conference on Stepping Motors and Systems*, September 1979: pp. 50-59.
- [2] Bringman, Matthew. *Finite Element Modeling of an 8/6 Switched Reluctance Machine for an Electromechanical Brake System*. Columbus: Ohio State University, 2001.
- [3] I.A. Khan. "Automotive Electrical Systems: Architecture and Components." Delphi Automotive Systems, Society of Automotive Engineers, 1998: pp. 11-12.
- [4] Keyhani, Ali. *Sizing Program for Switched Reluctance Motors*. Columbus: Ohio State University, 2000.
- [5] Lawernson, P.J., J.M. Stephenson, P.T. Blenkinsop, J. Corda, N.N. Fulton, Variable-Speed Switched Reluctance Motors." *Proceedings IEE*, vol. 127, Pt. B, no. 4, July 1980: pp.253-265.
- [6] Lipo, T.A., Surong Huang, Jian Luo, Franco Leonardi. "A General Approach to Sizing and Power Density Equations for Comparison of Electrical Machines." *IEEE Transaction on Industry Application*, vol. 34, no. 1, January/ February 1998.
- [7] Materu, P.N., Krishnan, R., "Estimation of switched reluctance motor losses." *IEEE Transactions on Industry Applications*, vol. 28, no. 3, pp. 668-679, May/June 1992.
- [8] Miller J.M., D. Goel, D. Kaminski, H.P. Schoner, T.M. Jahns. "Making the Case for a Next Generation Automotive Electrical System." Society of Automotive Engineers, 1998: pp. 1-9.
- [9] Miller, T.J.E., *Switched Reluctance Motors and Their Control*. Oxford: Magna Physics Publishing and Clarendon Press, 1993.

- [10] Moallem, M., H. Nikkhajoei, M. Falahi, "Predicting the Performance of a Switched Reluctance Machine Using Improved Magnetic Equivalent Circuit Method." IEEE, 1995.
- [11] Radun, Arthur. "Analytical Calculation of the Switched Reluctance Motor's Unaligned Inductance." *IEEE Transactions on Magnetics*, vol. 35, no. 6, November 1999.
- [12] Radun, Arthur. "Analytically Computing the Flux Linked by a Switched Reluctance Motor Phase When the Stator and Rotor Poles Overlap." *IEEE Transactions on Magnetics*, vol. 36, no. 4, July 2000.
- [13] Radun, Arthur V., "Design Considerations for the Switched Reluctance Motor." *IEEE Transactions on Industry Applications*, vol. 31, no. 5, September/October 1995.
- [14] Ramamurthy, Shyam S., Juan Carlos Balda. "Sizing a Switched Reluctance Motor for Electric Vehicles." *IEEE Transactions on Industry Applications*, vol. 37, no 5, September/October 2001.
- [15] Xu, Longya, Eric Ruckstadter. "Direct Modeling of Switched Reluctance Machine by Coupled Field-Circuit Method." *IEEE Transactions on Energy Conversion*, vol. 10, no. 3, September 1995.
- [16] Y. Hayashi and T.J.E. Miller. "A new approach to calculating core losses in the SR." *IEEE Transactions on Industry Applications*, vol. 31, no. 5, pp. 1039-1046, September/October 1995.